

Direct relationship between cell density and FDG uptake in asymptomatic aortic aneurysm close to surgical threshold: an in vivo and in vitro study

Cecilia Marini · Silvia Morbelli · Riccardo Armonino · Giovanni Spinella ·
Mattia Riondato · Michela Massollo · Francesca Sarocchi · Bianca Pane ·
Carla Augeri · Luca Abete · Giorgio Ghigliotti · Daniela Palmieri · Francesco Fiz ·
Giuseppe Cittadini · Ezio Fulcheri · Domenico Palombo · Gianmario Sambuceti

Received: 12 June 2011 / Accepted: 27 September 2011 / Published online: 20 October 2011
© Springer-Verlag 2011

Abstract

Purpose Conflicting results have been reported about the clinical value of fluorodeoxyglucose (FDG) imaging in predicting the risk of rupture of abdominal aortic aneurysm (AAA). The present study tests the hypothesis that FDG uptake is low in asymptomatic noninflammatory AAA due to the low cell density in aneurysmal walls.

Methods Positron emission tomography (PET)/CT imaging was performed in 12 consecutive candidates for AAA surgical repair and in 12 age- and sex-matched controls. At intervention, aneurysmal walls were cut into three sequential blocks. Block A was frozen to cut three 5- μ m slices for incubation with 2–3 MBq of FDG for 5 min. Block C was first incubated with the same tracer solution for the same time and subsequently frozen to cut three 5- μ m slices. Autoradiographic images were coregistered with immuno-

histochemical pictures of cell density, type and DNA synthesis as assessed on block B.

Results No visible uptake in abdominal aorta occurred in any patient or control subject. Immunohistochemistry documented a severe loss of wall structure, with low numbers of cells. Tracer retention directly correlated with overall cell density and with prevalence of cells synthesizing DNA. The metabolic nature of FDG uptake was confirmed by the selective effect of preliminary freezing that decreased tracer content by 90% in regions with high cell density and only by 34% in cold acellular areas.

Conclusion The loss of tissue structure and the marked decrease in cell density account for the low prevalence of positive findings at FDG PET imaging, at least in asymptomatic patients bearing AAAs whose diameter is close to surgical indication.

C. Marini (✉)
CNR Institute of Bioimaging and Molecular Physiology, Milan,
Genoa Section,
Genoa, Italy
e-mail: Cecilia.Marini@unige.it

S. Morbelli · R. Armonino · M. Riondato · M. Massollo ·
C. Augeri · F. Fiz · G. Sambuceti
Department Internal Medicine, Chair of Nuclear Medicine,
University of Genoa,
Genoa, Italy

G. Spinella · B. Pane · D. Palmieri · D. Palombo
Division of Vascular and Endovascular Surgery,
San Martino University Hospital, University of Genoa,
Genoa, Italy

F. Sarocchi · L. Abete · E. Fulcheri
Department of Surgical and Diagnostic Sciences, Pathology,
University of Genoa,
Genoa, Italy

G. Ghigliotti
Department of Internal Medicine, Chair of Cardiology,
University of Genoa,
Genoa, Italy

G. Cittadini
Department of Radiology, Hospital San Martino,
Genoa, Italy

C. Marini
Dipartimento di Neuroscienze,
Oftalmologia e Genetica dell'Università di Genova,
Via De Toni, 5,
16132 Genoa, Italy

Keywords Abdominal aortic aneurysm · Positron emission tomography/computed tomography · FDG uptake · Atherosclerosis

Introduction

Rupture is an acute and life-threatening complication of abdominal aortic aneurysm (AAA). Due to the effect of Laplace's law on arterial wall tension, its incidence increases in parallel with aortic diameter. Accordingly, surgery is currently indicated for aneurysms with diameter ≥ 5.5 cm [1]. However, even in AAAs of sub-threshold diameter (4.0–5.5 cm) the incidence of acute complications remains significant, ranging from 1 to 5% per year. Thus, risk stratification in these patients remains a major issue in vascular medicine and calls for a better capability to explore mechanisms underlying AAA acute complications. This task has been facilitated by both experimental and clinical studies documenting a relevant role for inflammatory infiltrates [1, 2] able to accelerate the proteolysis of elastin and collagen of aortic wall via the release of matrix metalloproteinases and proinflammatory cytokines [3–11].

These biological mechanisms recently gained renewed interest due to the capability of positron emission tomography (PET)/CT imaging with fluorodeoxyglucose (FDG) to highlight the insulin-independent glucose uptake of activated lymphocytes and macrophages infiltrating the diseased aortic segment [12–14]. However, more recent reports, including our own experience, were barely able to spot any visible FDG uptake in AAAs whose diameter size was just below the surgical threshold of 5.5 cm [15, 16].

Actually, pathological evidence suggests that the progressive increase in aneurysmal diameter is paralleled by a reduction in cell density [6] that might explain the inverse correlation between AAA size and FDG uptake with the possible confounding effect of nonspecific fluoride binding onto calcified arterial segments [17].

In the present study, we tested the hypothesis that with increasing AAA diameter cell density is too low to permit any visible FDG uptake. This limitation would particularly apply to asymptomatic patients bearing aortic dilatation with a size falling within a “grey zone” close to surgical indication but with uncertain therapeutic approach. For this purpose, we first tested the spatial agreement of radioactivity concentration with local cell density, type and mitotic activity by coregistering autoradiography with histological and immunohistochemical images. Then, to verify the specific nature of tracer binding, we tested the relationship between FDG uptake and glucose metabolism by modifying cell viability and biology via a preliminary freezing of aneurysmal samples.

Materials and methods

Patients

The study included 12 consecutive patients (10 men, 2 women, mean age 73 ± 5 , range 65–85 years) with asymptomatic AAA selected by the outpatient clinic of the Vascular and Endovascular Surgery Division of our University Hospital. All subjects were candidates for open surgical repair of AAA according to the evidence of diameter increase >10 mm in the last 6 months. The maximum anteroposterior aneurysm diameter was measured by CT and ranged from 45 to 53 mm (mean diameter 48 ± 3.5 mm) at the time of surgery. The main exclusion criteria included the presence of congestive heart failure, impaired renal function (serum creatinine >1.5 mg/dl), known intolerance to CT-iodinated contrast media or elevated blood glucose level (>130 mg/dl), significant concomitant diseases such as cancer, infections and, finally, autoimmune disorders.

Imaging data were compared with findings obtained in 12 age- and sex-matched subjects who were selected according to a case-control criterion among a population without cardiovascular risk factors or clinical evidence of cardiovascular disorders. All of these patients were submitted to PET/CT scan in the diagnostic workup of a suspected neoplastic disease. Patients previously submitted to either chemotherapy or radiotherapy, patients with aortic dilatation as well as patients with suspected autoimmune disease were excluded from the study. All patients signed the informed consent module to participate in the study that was approved by the local Ethics Committee.

Biochemical assays

Fasting blood samples were collected from all study subjects in the morning after resting in the supine position for 20 min during their outpatient clinical appointment. Plasma glucose, lipid and renal profile, total protein, serum fibrinogen, C-reactive protein (CRP) and N-terminal pro-brain natriuretic peptide (NT-proBNP) were assessed using standard techniques. Similarly, leukocyte and monocyte counts were measured using automated cell counters.

PET/CT acquisition

After a 12-h fast, serum glucose level was measured before the intravenous injection of 4.8–5.2 MBq of FDG per kilogram of body weight. All of these procedures were performed 4–10 days before surgery, with the patient recumbent in a supine position in a quiet room and instructed not to move. FDG PET imaging, from the skull base to the femoral neck, started 60–90 min after tracer

injection and was performed using an integrated PET/CT scanner characterized by a PET spatial resolution of 4 mm full-width at half-maximum (Hi-REZ, Siemens Medical Solutions, Knoxville, TN, USA).

CT aortic angiography was performed within 1 week from the FDG PET study using the same 16-slice CT scanner. Patients were placed in a supine position, and topograms in the anteroposterior view were obtained from the diaphragm to the pelvis. Intravenous contrast medium was injected into an antecubital vein, using an automatic injection system via a 20-gauge cannula. Synchronization between the passage of contrast and baseline arterial phase was conducted in real time using an automatic fire detection system on the upper abdominal aorta (Bolus Tracking, Siemens Medical Solutions, Erlangen, Germany). The control sequence was activated 10 s after the start of contrast injection and implied the acquisition of one image every second. The start of the study was triggered automatically when the intensity level of contrast reached 180 HU, within a region of interest (ROI) placed on the abdominal aorta. In all cases, the craniocaudal direction was used.

In vivo image analysis

PET raw data were reconstructed by means of ordered subset expectation maximization (OSEM) and attenuation correction was performed using the CT raw data. The entire CT data set was fused with the three-dimensional PET images using an integrated software interface (Syngo Image Fusion, Siemens Medical Solutions, Erlangen, Germany) to create anatomical images superimposed with FDG uptake in the investigated body districts.

Volumetric regions of interest (VROIs) were placed on the anatomical CT images to identify four aortic segments (ascending, arch, descending and abdominal aorta), common carotid arteries and iliac arteries. In the case of bilateral branches, the mean value was considered. Two further VROIs were drawn in the liver and in the left ventricular chamber using the PET image to estimate liver uptake and arterial tracer concentration, respectively. Finally, in all patients with AAA, an additional VROI was drawn over the aneurysmal arterial walls.

FDG uptake was quantified by the maximum standardized uptake value (SUV) within each VROI according to the recently published guidelines [18]. To account for the contribution of blood FDG activity, all SUVs were divided by the corresponding value in the blood pool as proposed by Rudd et al. [19, 20]. In no case was correction for partial volume effect attempted due to the absence of clearly visible areas of focal uptake within the analysed vascular segments [21].

The degree of arterial calcification was measured from the takeoff of renal arteries to bifurcation of aorta into

common iliac arteries. For this purpose, we used a dedicated software (OsiriX) providing Agatston scores whose values were adjusted to account for slice width as previously published by Ellison et al. [22]. In the aneurysmal walls, arterial calcium load was estimated according to the semiquantitative method proposed by Siegel et al. [23]. For this purpose, two independent observers, blinded to the patient status, were asked to grade calcium density according to a semiquantitative 5-point scale based on per cent calcification of the arterial ring documented in the transaxial views: (0=no calcific deposits, 1=0–25%, 2=25–50%, 3=50–75% and 4=75–100%).

Autoradiographic analysis of abdominal aneurysmal artery samples

At the time of the surgical repair, the biodistribution of FDG within the aortic tissue was studied with digital autoradiography. Immediately after harvesting, the aneurysmal abdominal aorta was taken to the pathology lab of our hospital. The specimen was dissected, blood was washed with saline and the surrounding connective tissue and fat were removed. The AAA sample was then divided into three sequential blocks, from A to C. Blocks A and C were used for autoradiography, while block B was submitted to immunohistochemistry. The thickness of each block ranged from 3 to 5 mm for a weight of 150–450 mg.

Block A was frozen in isopentane chilled with dry ice for sectioning with a cryomicrotome, according to the procedure described by Laitinen et al. [17]. Starting from the cutting border with block B, a minimum of three sequential sections were cut at -15°C and thaw-mounted onto microscope slides. Slice thickness was set at 5 μm to optimize image spatial resolution. The sections were then warmed to room temperature, incubated in saline for 20 min and, thereafter, immersed in 20 ml of saline containing 2–3 MBq/ml of FDG for 30 min. Thus, the slices were washed twice with ice-cold saline, rinsed in distilled water and air-dried (with a hair dryer for 10 min).

By contrast, the whole fresh block C was first incubated in the same tracer solution, for the same time and under the same experimental conditions used for the sections from block A. Thus, the specimen was washed, dried and then frozen in isopentane chilled with dry ice for sectioning with the cryomicrotome with the same procedure used for block A, again obtaining a minimum of three sequential sections, 5 μm thick, starting from the cutting border with block B.

Thereafter, all slides were exposed to an imaging plate (Cyclone, PerkinElmer Analysis Facilities) that provides an image resolution of 50 μm . Different times of exposure were sequentially utilized in all experiments: 2, 5, 15, 30 and 60 min. At the end of the procedure, all aortic sections were stained using the haematoxylin and eosin technique.

Autoradiographic image analysis

Plates were scanned and images were analysed for count densities (photostimulated luminescence per unit area, PSL/mm²) with a dedicated image analysis software (OsiriX). For this purpose, a minimum of four ROIs were manually drawn in each image to identify hot and cold areas, respectively. Each region was thus saved to be exported for blind histological analysis.

For freshly incubated specimens, an exposure to the imaging plate longer than 5 min systematically prevented the analysis of FDG distribution due to saturation effect. On the contrary, for previously frozen slices, an exposure time shorter than 30 min consistently prevented an adequate analysis due to poor image statistics.

FDG uptake in samples incubated before or after freezing was estimated by comparing the number of PSD (counts) normalized for the different acquisition times (5 vs 30 min) and the consequent effect of ¹⁸F physical decay, according to the conventional formulations.

Histology

The central block B was fixed in 10% formalin solution and embedded in paraffin to optimize immunohistochemical analysis. Thereafter, two series of five—5 μm thick—paraffin sections were obtained, starting from both cutting borders facing toward either block A and block C. This procedure ensured that each autoradiography, regardless of its provenience, had a direct immunohistochemical counterpart obtained in the adjacent tissue.

Starting from each cutting border, block B sections were always stained, according to the same order, to allow the sequential analysis of the following variables: (1) tissue structure, (2) cells under any phase of active cell cycle, (3) leukocyte nature of cellular infiltrates and, finally, (4) T and B lymphocytes.

No histological analysis was performed on autoradiography slices to avoid the relative loss in image quality affecting previously frozen sections. Immunohistochemistry evaluation was performed using a panel with CD3 (Ventana), CD20 (Ventana) and Ki-67/MIB-1 (Dako) antibodies, in a ready-to-use formulation, on the paraffin-embedded and formalin-fixed slides. The standard avidin-biotin complex technique was employed for all immunostains; antibodies were optimized for use on an automated slide stainer in combination with Ventana detection kits. Heat pretreatment (microwave) and endogenous biotin blocking were performed for all of the above-mentioned antibodies. Finally, all slides were counterstained with haematoxylin for 4 min.

A report was completed by two experienced pathologists, who described the specimens on a standard reporting form that included degree of atherosclerosis (graded 0–3)

[8], plaque and vessel calcification as well as degree of medial and adventitial inflammation (density of inflammatory cells). For the coregistration study, pathology readers were blinded to the results of autoradiography and, in particular, were left unaware of ROI nature (hot or cold). ROI borders, saved in TIFF format, were reported on all of the histological images formatted in the same matrix.

Statistical analysis

Intergroup differences in maximal arterial SUV were tested in each vascular segment using Student's *t* test for unpaired data. Intersegment variability in arterial SUV was tested in each patient using the *t* test for paired data and Bonferroni correction. Linear regression analysis was performed using the least-squares method. A *p* value <0.05 was considered significant.

Results

Clinical data

The main clinical and metabolic characteristics were similar in patients and controls as reported in Tables 1 and 2, respectively. Surgical intervention was successfully completed in all patients and no complication in the postoperative period occurred. An AAA example is reported in Fig. 1, where the image fusion of CT angiography and FDG PET clearly shows, on one side, the vascular dilatation associated with the presence of calcium load and, on the other, the low metabolic activity of the aneurysmal walls.

PET/CT evaluation of AAA

The main descriptors of systemic FDG kinetics did not differ in the two populations. In fact, the average SUV was

Table 1 Demographics and treatment of study subjects

	AAA patients (<i>n</i> =12)	Controls (<i>n</i> =12)
Age (years)	73±5	73±4
M/F	11/1	11/1
Body mass index (kg/m ²)	24.5±0.4	22.2±0.4
History of smoking (%)	10/12 (83%)	7/12 (58%)
Hypertension (%)	11/12 (92%)	8/12 (67%)
Hypercholesterolaemia (%)	8/12 (67%)	–
ACE 1 or AT1 inhibitors (%)	10/12 (83%)	6/12 (50%)
β-Blockers (%)	2/12 (17%)	1/12 (8%)
Aspirin or ticlopidine (%)	11/12 (92%)	5/12 (42%)
Lipid-lowering drugs (%)	6/12 (50%)	–

Table 2 Laboratory tests of study patients

	AAA patients (n=12)	Controls (n=12)
Blood glucose (mg/dl)	96.2±9.0	88±12
Total serum cholesterol (mg/dl)	176.4±14.6	–
Triglycerides (mg/dl)	84±12	–
Uric acid (mg/dl ⁻¹)	5.4±0.4	–
Creatinine (mg/dl ⁻¹)	1.02±0.11	0.96±0.14
Total protein (g/dl ⁻¹)	7.8±0.2	–
Serum fibrinogen (mg/dl ⁻¹)	327±50	–
CRP (mg/l ⁻¹)	6.4±4.1	–
NT-proBNP (pg/ml)	118±57.2	–
White blood cell count (mm ⁻³)	6,943±411	6,712±582
Neutrophil count (mm ⁻³)	4,712±264	4,221±291
Monocyte count (mm ⁻³)	452±71	411±62

similar in patients and in controls both in liver (2.2±0.4 vs 2.1±0.5, respectively, *p*=NS) and in left ventricular blood (2.0±0.5 vs 2.1±0.6, respectively, *p*=NS). As shown in Fig. 2, no differences were observed in glucose metabolism in all non-diseased segments of aorta, common carotid arteries and iliac branches in the two groups. On the contrary, aneurysmal FDG uptake was significantly lower with respect to the corresponding arterial regions of control subjects (0.91±0.16 vs 1.54±0.39, respectively, *p*<0.01, Fig. 2). Compared to control subjects, AAA patients showed no significant differences in calcium load both in the whole infrarenal abdominal aorta (modified Agatston

score: 3,845±2,000 vs 3,595±1,461, respectively, *p*=NS) and in the aneurysmal segment (semiquantitative scoring system: 2.9±1.2 vs 2.4±1.1, respectively, *p*=NS).

Autoradiographic features of aortic aneurysm

Independently of sample processing protocol, overall FDG distribution was largely heterogeneous with spots of clearly visible radioactivity surrounded by large areas characterized by low tracer content. Thrombi, when present, were always characterized by the absence of any visible radioactivity.

The different processing protocols resulted in marked differences in glucose metabolism. Despite the fact that the two samples were incubated with the same tracer solution for an identical incubation time, the history of recent transient freezing decreased FDG uptake by almost 8 times in hot regions, i.e. from 30.5±8.7×10³ PSL/mm² min⁻¹ (in freshly incubated samples) to 3.7±1.1×10³ PSL/mm² min⁻¹ (in previously frozen specimens, respectively, *p*<0.001). On the contrary, in cold areas tracer retention accounted for 3.5±0.9×10³ PSL/mm² min⁻¹ vs 1.9±0.9×10³ PSL/mm² min⁻¹ in fresh and previously frozen samples, respectively (*p*<0.001).

Thus, after the thermal shock, FDG uptake dramatically decreased by 87±5% within hot regions and by only 34±35% in the cold ones (*p*<0.001). This differential effect obviously affected image quality by modifying the tracer distribution throughout the slice. In fact, the ratio between hot and cold areas was 9.2±2.7 in freshly incubated samples vs 2.2±0.7 in previously frozen ones (*p*<0.001).

Fig. 1 Left panels display 3-D reconstructions of PET/CT data and document the absence of any visible FDG uptake in the abdominal aortic region. CT transaxial plane (bottom, centre panel) displays the presence of an aortic aneurysm that is partially occupied by thrombotic material as documented by contrast CT angiography as well as by the absence of any visible FDG uptake at PET/CT coregistration. Right panels display the 3-D reconstructions of CT aortic angiography showing the aneurysmal portion as indicated by the green arrows

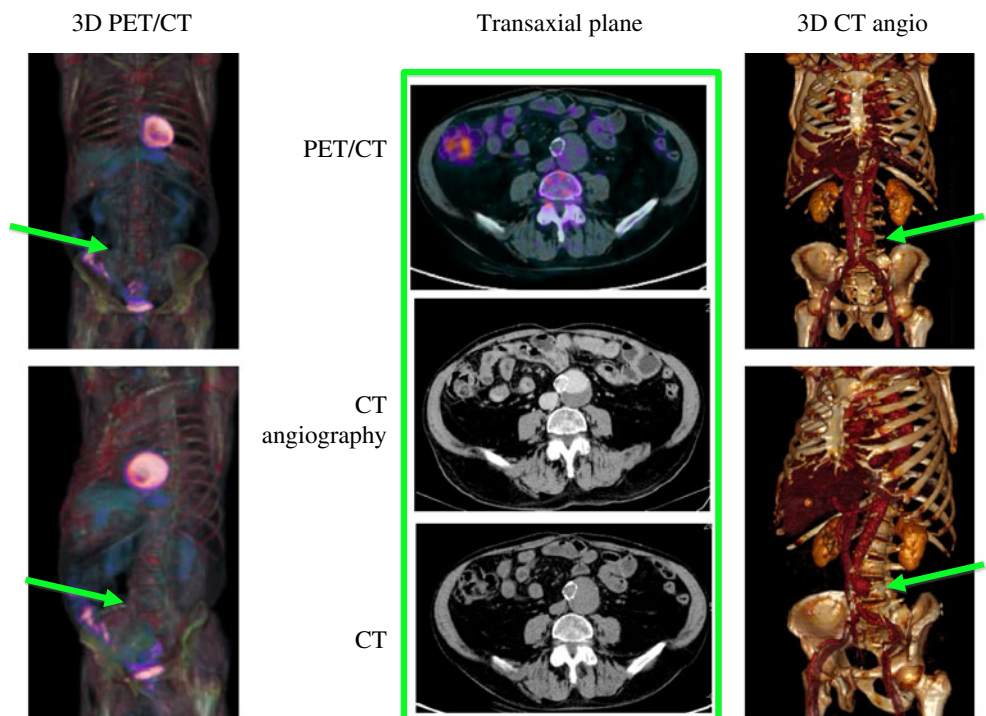
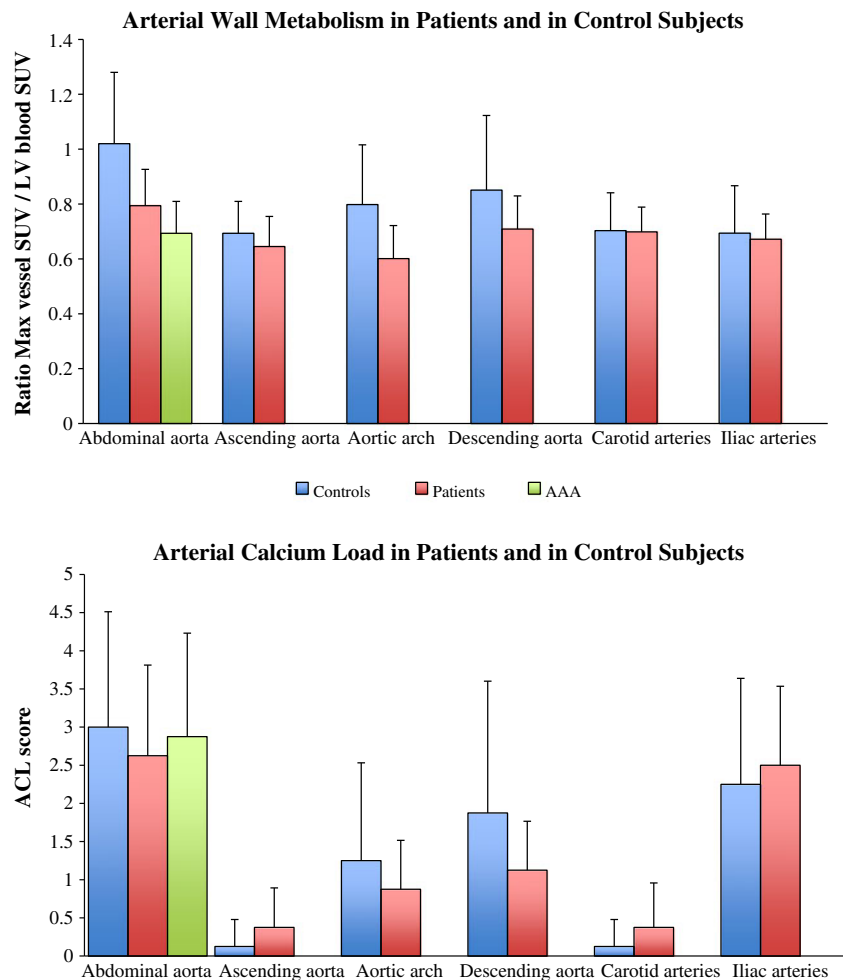


Fig. 2 *Top panel* displays SUVs in the different arterial segments of patients and control subjects. The SUV was similar in all vascular segments in both groups (*blue and red columns*, respectively). Interestingly, FDG uptake was significantly lower in aneurysmal aortic segments with respect to controls subjects (*green column*). *Bottom panel* displays total calcium load (*ACL*) that was similar in patients and in control subjects



Histological correlates of FDG uptake in aortic aneurysm

Aneurysm samples showed evidence of extensive atherosclerosis, graded 2–3, in all biopsies with necrosis, lipid deposits and/or calcifications. Evidence of ulcerated plaque occurred in 10 of 12 cases within the anatomical piece. Adhesive thrombus within the histological specimen occurred in 6 of 12 patients.

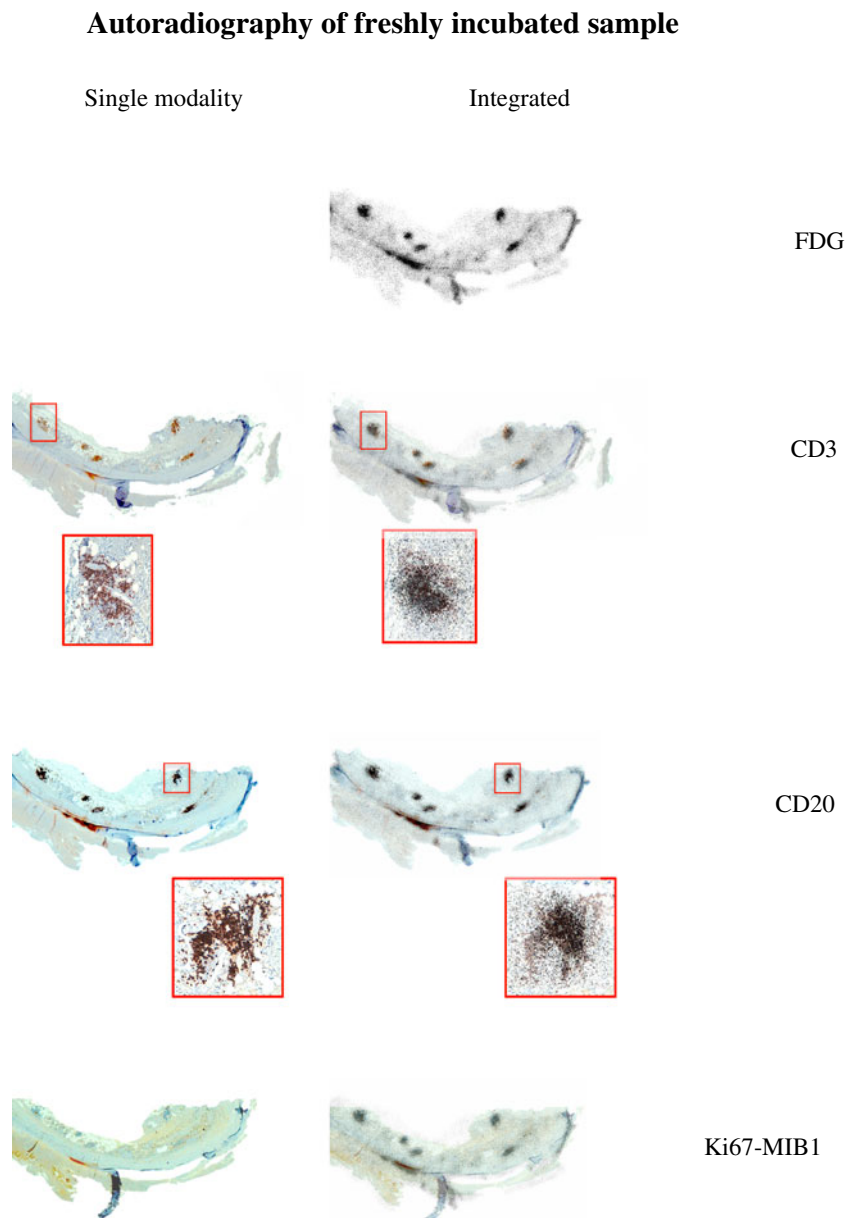
Haematoxylin and eosin staining of AAA specimens documented a loss of wall structure and a marked reduction in overall cell density. As expected, histological analysis documented a moderate inflammatory infiltration that encompassed the entire arterial wall although it was particularly evident in its outer layers. Representative examples of the extent of arterial wall inflammation are shown in Fig. 3. Immunohistochemistry showed that the majority of cells (>85%) in both adventitia and media were leukocytes as documented by CD45 staining in all cases, with a striking prevalence of CD3 and CD20 lymphocytes (>80%). On the contrary, granulocytes and macrophages were rarely found. Prevalence of cells in all phases of the

active cycle was documented by Ki-67 expression and was $4.6 \pm 3\%$. There was no evidence of bacteria or other unusual findings in any biopsies.

At coregistration analysis, the difference in tracer uptake was paralleled by an even more evident gap in cell density that was ten times higher in hot areas with respect to the cold ones without any differences between the two protocols (227 ± 67 vs 27 ± 21 cells/mm² in fresh samples, 212 ± 70 vs 16 ± 8 cells/mm² in frozen samples, respectively, $p < 0.001$). Moreover, all regions without any evidence of cells were observed in cold ROIs. Similarly, the prevalence of cells actively synthesizing DNA, documented by their Ki-67 expression, was remarkably higher in hot than in cold regions both in freshly incubated samples ($10 \pm 3\%$ vs $1.8 \pm 0.1\%$, respectively, $p < 0.01$) and in slices incubated after freezing ($8.3 \pm 3\%$ vs $1.4 \pm 0.6\%$, $p < 0.01$).

Finally, as shown in Fig. 4, a direct correlation was documented in each ROI between FDG concentration and density of both overall cells and cells in all phases of the active proliferation cycle. These correlations were more clearly evident for data obtained after incubation of fresh

Fig. 3 Immunohistochemical and autoradiographic analysis of a pathological sample of aortic aneurysm, incubated with FDG before cryotome application. *Top right panel* displays the autoradiographic image obtained from a slice cut from block C at its border with block B. *Left panels* display the immunohistochemical images of three sequential slices obtained after fixation from block B at its cutting border with block C. At the right of each image, its coregistration with autoradiography is shown. Starting from the top each row displays T lymphocytes recognized by CD3 staining, B lymphocytes identified on the basis of CD20 positivity and cells actively synthesizing DNA documented by Ki-67 expression. Despite the fact that these four images reflect the distribution of each marker in four sequential 5- μ m thick slices, the close agreement between cell density and metabolic activity is evident on the *right panels* and is confirmed by the details shown for the first two rows. Original magnification $\times 200$



sample with respect to those provided by previously frozen slices.

Discussion

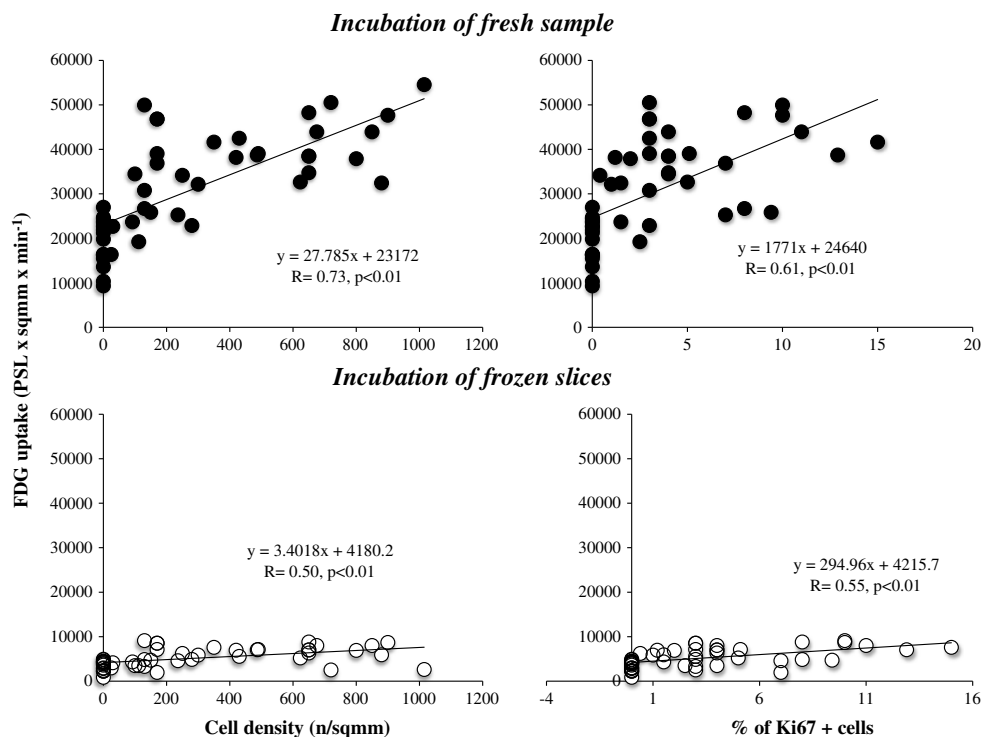
The present study used an in vitro method to explain the low prevalence of positive findings at FDG PET imaging of asymptomatic AAAs with a size close to surgical indication. At this stage, diseased aortic walls typically display a marked reduction in cell density. Autoradiographic evaluation showed that radioactivity content was prevalently confined to populated islets being instead virtually absent in the residual, largely acellular, regions. The exposure to a

transient thermal shock profoundly decreased cell tracer uptake, having only minor effect on the remaining acellular tissue. Altogether these data directly document that FDG retention accurately tracks glucose uptake being only modestly affected by unspecific binding. Accordingly, the extremely low FDG retention in these relatively large asymptomatic AAAs reflects the metabolic activity of an extremely low number of cells present within diseased arterial walls.

Biological bases of FDG PET imaging in AAA patients

The capability of PET to visualize FDG uptake in vulnerable atherosclerotic plaques [24, 25] or large vessel vasculitis [26]

Fig. 4 Correlation between count density in each ROI and number of overall cells (*left*) or prevalence of Ki-67 elements (*right*). Immediate incubation after harvesting (*top panels, solid circles*) resulted in a markedly higher tracer uptake with respect to exposure to FDG after the thermal shock of cryomicrotome (*bottom, circles*). Despite this difference, a significant correlation was still observed between histological indicators of cell pattern and tracer uptake for both experimental protocols



has already been documented. On the contrary, the clinical value of this tool in asymptomatic AAA patients is less clear, since the high prevalence of positive scans in preliminary studies has not been confirmed by more recent reports [15, 16]. This variability agrees with the current model of AAA progression [27, 28] characterized by the repetitive sequence of inflammatory damage and repair. However, when arterial diameter reaches values close to surgical indications, cell density is eventually reduced throughout the aneurysmal walls [4–6, 29, 30]. This sequence of events might thus imply a cyclic variation in FDG uptake in early stages and a progressive reduction of tracer retention in later ones. Accordingly, positive PET findings should be more frequently encountered in aneurysms of small size or in those involved in large inflammatory processes that are more frequently associated with symptoms and require direct surgical repair [12].

The micrometric analysis of FDG distribution and its coregistration with histology strongly corroborates this interpretation of the mechanisms underlying the reduced tracer retention in the diseased arterial segment. In fact, FDG uptake was extremely heterogeneous within the damaged arterial wall, with regions characterized by a “relatively preserved” metabolism clearly visible in the low background of the remaining vascular tissue. Metabolically inert areas were consistently located in fibrotic tissue, in endoluminal thrombus or in necrotic regions. These metabolic features agree with the pathological peculiarities of uncomplicated AAA characterized by the loss of smooth muscle cells [6] and by the

presence of infiltrating lymphocytes [4, 5] in contrast to the higher cell number and macrophage infiltration found in occlusive atherosclerosis [24] or in symptomatic AAAs complicated by inflammation [12].

This concept is further corroborated by the coregistration of autoradiography with immunohistochemistry: FDG uptake closely correlated with the number of lymphocytes under active mitotic cycle as documented by Ki-67 staining [31]. Thus, this in-depth analysis of tracer handling by aneurysmal walls indicates that FDG actually tracks the local glucose consumption. However, the overall number of cells entrapping this tracer is excessively low to permit the *in vivo* diagnosis of AAA inflammation, at least in these asymptomatic patients, whose arterial dilatation falls in a grey zone close to surgical indication. This clinical condition might thus be better approached by evaluating more specific molecular pathways. In this line, the high prevalence of lymphocytes in cellular infiltrates of diseased walls might represent the basis for imaging with tracer targeted to interleukin 2 [32].

Methodological considerations

The technique of autoradiography is most often used to evaluate the distribution of tracers after their *in vivo* injection. However, under many experimental conditions, a direct incubation of biological samples is needed to verify the tissues responsible for tracer uptake. In this setting, specimen physiology responds to an artificial environment

in which signalling systems modulating cellular metabolism are lacking, oxygen tension is not preserved due to the absence of perfusion while tracer concentration remains relatively stable throughout the incubation period. Due to these considerations, this procedure does not permit testing of possible quantitative correlations between *in vitro* FDG uptake and *in vivo* SUV. On the contrary, it permits one to accurately verify the spatial distribution of the metabolic tracer within the analysed tissue.

In vitro autoradiography can be performed according to two procedures: direct incubation of tissue sample and subsequent freezing for slice preparation [29–32] or preliminary freezing and sectioning followed by slice incubation [17, 33, 34]. The former protocol offers the advantage of a relatively preserved physiology of the experimental specimen. The latter procedure [17] permits exposure of all cells to the same tracer concentration, thus avoiding the possible presence of gradients between inner and outer layers that can occur in a freshly incubated sample. Although incubation of previously frozen slices improves the accuracy of receptor binding studies [33, 34], the exposure to a thermal shock profoundly disrupts cellular biology and viability hampering the link between FDG uptake and glucose metabolism. In this line, preliminary freezing can be considered as a tool to estimate the contribution of unspecific tracer binding to the overall FDG distribution in analysed tissue. Cell tracer content eventually decreased to less than 15% in previously frozen slices with respect to values measured after incubation of the corresponding fresh specimen. On the contrary, preliminary freezing only modestly modified the radioactivity counts of necrotic and fibrotic regions. Thus, the selectivity of thermal shock effect documents that contamination from unspecific tracer binding plays a minor role in overall AAA FDG uptake. This finding extends previous observations reporting a high tracer uptake in acellular calcified regions in aortic specimens previously submitted to snap freezing [17]. In this line, tracer uptake in AAA walls reflects both specific (metabolic) and unspecific binding mechanisms. The relative contribution of these two different pathways varies according to the stage of the lesion and thus to its cell density.

Limitations

Aortic dilatation remains most often asymptomatic throughout its progression until it reaches a size that requires intervention. This usually precludes obtaining fresh specimens of uncomplicated AAA in earlier disease stages. Therefore, we cannot extend the present observations to describe the natural history of AAA progression. Similarly, the present study does not elucidate the potential of PET/CT imaging of FDG distribution in predicting aneurysm inflammation and risk of rupture in patients with aneurysms

of relatively smaller size presenting with suspicious but non-diagnostic clinical features.

However, the present study was planned to identify the biological mechanisms underlying FDG uptake in uncomplicated, asymptomatic AAA. In this line, the consistent nature of our findings, as well as their agreement with clinical studies in larger populations [16], permit us to explain the reason why asymptomatic patients with a relatively large aneurysm most often present an extremely low FDG uptake at PET imaging.

In the present study, immunohistochemical evaluation of diseased aorta did not include CD68 staining to recognize macrophage infiltration. This selection was motivated by the evidence that the large majority of infiltrating cells (>80%) were lymphocytes. This finding agrees with the inclusion criteria that aimed to exclude patients with suspected AAA inflammation. In this line, the evidence of such a large lymphocyte presence in asymptomatic AAA suggests these cells play a role in the natural history of the disease, even in phases not characterized by active inflammation.

Finally, the heterogeneous nature of cell populations in AAA specimens might partially reduce the agreement of data collected from different slices. This procedure was motivated by the fact that the short half-life of ^{18}F implies an almost immediate imaging of its distribution, while immunohistochemistry requires a long fixation time to obtain accurate image definition. To improve the accuracy of the coregistration procedure, great care was paid to ensure the contiguity of the slices submitted to autoradiography and immunohistochemistry. As a result, the correlation between tracer concentration and cell density was indeed robust enough as to document that FDG retention is modulated by its well-known determinants, i.e. local glucose uptake as an indirect index of cell density and metabolic activation.

Conclusion

AAA is the end result of a multifactorial process that is characterized by the progressive loss of cell populations associated with an irreversible remodelling of the arterial connective tissue eventually culminating in aortic rupture. These pathways are extremely complex and probably vary in the different disease stages. According to this concept, in AAAs whose size reaches a relatively large diameter, cell density is decreased to levels so low as to prevent any visible FDG uptake.

The match between FDG behaviour and cell density confirms this concept and offers a good explanation of the extremely low prevalence of “positive” PET/CT scans in these patients. Obviously, this pathological picture is just one snapshot in time and may not be representative of all

pathophysiological mechanisms underlying aortic rupture or progressive dilatation. These data therefore corroborate the concept that PET/CT imaging might not represent an accurate screening tool to identify rupture risk in these asymptomatic patients. In particular, the profound agreement between cell density and FDG uptake suggests that care should be taken in considering a negative PET scan as an index of low risk. As AAA diameter enlarges, in fact, the marked loss of cells and tissue structure within the diseased walls might increase the risk of rupture caused by mechanical stressors and amplified by aortic dilatation.

Conflicts of interest None.

References

- Ballard DJ, Filardo G, Fowkes G, Powell JT. Surgery for small asymptomatic abdominal aortic aneurysms. *Cochrane Database Syst Rev* 2008;4:CD001835.
- Lederle FA. Abdominal aortic aneurysm—open versus endovascular repair. *N Engl J Med* 2004;351:1677–9.
- Anidjar S, Salzman JL, Gentric D, Lagneau P, Camilleri JP, Michel JB. Elastase-induced experimental aneurysms in rats. *Circulation* 1990;82:973–81.
- Ocana E, Bohórquez JC, Pérez-Requena J, Brieva JA, Rodríguez C. Characterisation of T and B lymphocytes infiltrating abdominal aortic aneurysms. *Atherosclerosis* 2003;170:39–48.
- Koch AE, Haines GK, Rizzo RJ, Radosevich JA, Pope RM, Robinson PG, et al. Human abdominal aortic aneurysms. Immunophenotypic analysis suggesting an immune-mediated response. *Am J Pathol* 1990;137:1199–213.
- Henderson EL, Geng Y-J, Sukhova GK, Whittemore AD, Knox J, Libby P. Death of smooth muscle cells and expression of mediators of apoptosis by T lymphocytes in human abdominal aortic aneurysms. *Circulation* 1999;99:96–104.
- Koch AE, Kunkel SL, Pearce WH, Shah MR, Parikh D, Evanoff HL, et al. Enhanced production of the chemotactic cytokines interleukin-8 and monocyte chemoattractant protein-1 in human abdominal aortic aneurysms. *Am J Pathol* 1993;142:1423–31.
- Freestone T, Turner RJ, Coady A, Higman DJ, Greenhalgh RM, Powell JT. Inflammation and matrix metalloproteinases in the enlarging abdominal aortic aneurysm. *Arterioscler Thromb Vasc Biol* 1995;15:1145–51.
- Goodall S, Crowther M, Hemingway DM, Bell PR, Thompson MM. Ubiquitous elevation of matrix metalloproteinase-2 expression in the vasculature of patients with abdominal aneurysms. *Circulation* 2001;104:304–9.
- Carrell TW, Burnand KG, Wells GM, Clements JM, Smith A. Stromelysin-1 (matrix metalloproteinase-3) and tissue inhibitor of metalloproteinase-3 are overexpressed in the wall of abdominal aortic aneurysms. *Circulation* 2002;105:477–82.
- Annabi B, Shédid D, Ghosn P, Kenigsberg RL, Desrosiers RR, Bojanowski MW, et al. Differential regulation of matrix metalloproteinase activities in abdominal aortic aneurysms. *J Vasc Surg* 2002;35:539–46.
- Reeps C, Essler M, Pelisek J, Seidl S, Eckstein HH, Krause BJ. Increased 18F-fluorodeoxyglucose uptake in abdominal aortic aneurysms in positron emission/computed tomography is associated with inflammation, aortic wall instability, and acute symptoms. *J Vasc Surg* 2008;48:417–23.
- Kotze CW, Menezes LJ, Endozo R, Groves AM, Ell PJ, Yusuf SW. Increased metabolic activity in abdominal aortic aneurysm detected by 18F-fluorodeoxyglucose (18F-FDG) positron emission tomography/computed tomography (PET/CT). *Eur J Vasc Endovasc Surg* 2009;38:93–9.
- Sakalihan N, Hustinx R, Limet R. Contribution of PET scanning to the evaluation of abdominal aortic aneurysm. *Semin Vasc Surg* 2004;17:144–53.
- Truijers M, Kurvers HAJM, Bredie SJH, Oyen WJG, Blankensteijn JD. In vivo imaging of abdominal aortic aneurysms: increased FDG uptake suggests inflammation in the aneurysm wall. *J Endovasc Ther* 2008;15:462–7.
- Palombo D, Morbelli S, Spinella G, et al. A positron emission/computed tomography (PET/CT) evaluation of asymptomatic abdominal aortic aneurysms: another point of view. *Ann Vasc Surg* 2011; in press.
- Laitinen I, Marjamäki P, Haaparanta M, Savisto N, Laine VJ, Soini SL, et al. Non-specific binding of [18F]FDG to calcifications in atherosclerotic plaques: experimental study of mouse and human arteries. *Eur J Nucl Med Mol Imaging* 2006;33:1461–7.
- Boellaard R, O'Doherty MJ, Weber WA, Mottaghy FM, Lonsdale MN, Stroobants SG, et al. FDG PET and PET/CT: EANM procedure guidelines for tumour PET imaging: version 1.0. *Eur J Nucl Med Mol Imaging* 2010;37:181–200.
- Rudd JH, Myers KS, Bansilal S, Machac J, Rafique A, Farkouh M, et al. (18)Fluorodeoxyglucose positron emission tomography imaging of atherosclerotic plaque inflammation is highly reproducible: implications for atherosclerosis therapy trials. *J Am Coll Cardiol* 2007;50:892–6.
- Rudd JH, Myers KS, Bansilal S, Machac J, Pinto CA, Tong C, et al. Atherosclerosis inflammation imaging with 18F-FDG PET: carotid, iliac, and femoral uptake reproducibility, quantification methods, and recommendations. *J Nucl Med* 2008;49:871–8.
- Izquierdo-Garcia D, Davies JR, Graves MJ, Rudd JH, Gillard JH, Weissberg PL, et al. Comparison of methods for magnetic resonance-guided [18-F]fluorodeoxyglucose positron emission tomography in human carotid arteries: reproducibility, partial volume correction, and correlation between methods. *Stroke* 2009;40:86–93.
- Ellison JC, Zhang Y, Wagenknecht LE, Eckfeldt JH, Hopkins PN, Pankow RS, et al. Relation of the metabolic syndrome to calcified atherosclerotic plaque in the coronary arteries and aorta. *Am J Cardiol* 2005;95:1180–6.
- Siegel CL, Cohan RH, Korobkin M, Alpern MB, Courmeyra DL, Leder RA. Abdominal aortic aneurysm morphology: CT features in patients with ruptured and nonruptured aneurysms. *AJR Am J Roentgenol* 1994;163:1123–9.
- Rudd JH, Warburton EA, Fryer TD, Jones HA, Clark JC, Antoun N, et al. Imaging atherosclerotic plaque inflammation with [18F]-fluorodeoxyglucose positron emission tomography. *Circulation* 2002;105:2708–11.
- Ogawa M, Ishino S, Mukai T, Asano D, Teramoto N, Watabe H, et al. (18)F-FDG accumulation in atherosclerotic plaques: immunohistochemical and PET imaging study. *J Nucl Med* 2004;45:1245–50.
- Walter MA, Melzer RA, Schindler C, Müller-Brand J, Tyndall A, Nitzsche EU. The value of [18F]FDG-PET in the diagnosis of large-vessel vasculitis and the assessment of activity and extent of disease. *Eur J Nucl Med Mol Imaging* 2005;32:674–81.
- van der Vliet JA, Boll AP. Abdominal aortic aneurysm. *Lancet* 1997;349:863–6.
- Daugherty A, Cassis LA. Mechanisms of abdominal aortic aneurysm formation. *Curr Atheroscler Rep* 2002;4:222–7.

29. Satta J, Laurila A, Pääkko P, Haukipuro K, Sormunen R, Parkkila S, et al. Chronic inflammation and elastin degradation in abdominal aortic aneurysm disease: an immunohistochemical and electron microscopic study. *Eur J Vasc Endovasc Surg* 1998;15:313–9.
30. Stella A, Gargiulo M, Pasquinelli G, Preda P, Faggioli GL, Cenacchi G, et al. The cellular component in the parietal infiltrate of inflammatory abdominal aortic aneurysms (IAAA). *Eur J Vasc Surg* 1991;5:65–70.
31. Tisell LE, Oden A, Muth A, Altiparmak G, Mölne J, Ahlman H, et al. The Ki67 index a prognostic marker in medullary thyroid carcinoma. *Br J Cancer* 2003;89:2093–7.
32. Annovazzi A, Bonanno E, Arca M, D'Alessandria C, Marcoccia A, Spagnoli LG, et al. ^{99m}Tc-interleukin-2 scintigraphy for the in vivo imaging of vulnerable atherosclerotic plaques. *Eur J Nucl Med Mol Imaging* 2006;33:117–26.
33. Zubal G, Fujibayashi Y, Maruoka N, Omata N, Yonekura Y. Automated kinetic analysis of FDG uptake in living rat brain slices from dynamic positron autoradiography. *Cancer Biother Radiopharm* 2003;18:405–11.
34. Colin S, Mascarelli F, Jeanny JC, Vienet R, Bouche G, Courtois Y, et al. Comparative study in vivo and in vitro of uniformly ¹⁴C-labelled and ¹²⁵I-labelled recombinant fibroblast growth factor 2. *Eur J Biochem* 1997;249:473–80.